N-cadherin facilitates trigeminal sensory neuron outgrowth and target tissue innervation

Caroline A. Halmi[1], Carrie E. Leonard[1], Alec T. McIntosh[2] Lisa A. Taneyhill[1,*]

[1]Department of Animal and Avian Sciences, University of Maryland, College Park, MD 20742 USA

[2]Lombardi Comprehensive Cancer Center, Georgetown University, Washington, DC, 20007 USA

*Lisa A. Taneyhill

Email: ltaney@umd.edu

Keywords: Trigeminal ganglion, neural crest, placode cells, and N-cadherin.

ABSTRACT

During embryonic development, diverse cell types coordinate to form functionally complex tissues. Exemplifying this process, the trigeminal ganglion emerges from the condensation of two distinct precursor cell populations, cranial placodes and neural crest, with neuronal differentiation of the former preceding the latter. While its dual cellular origin has been understood for decades, the molecules orchestrating trigeminal ganglion formation remain relatively obscure. Initial assembly of the trigeminal ganglion is mediated by cell adhesion molecules, including neural cadherin (N-cadherin), which is first expressed by placodal neurons and is required for their proper condensation with other neurons and neural crest cells. Axon outgrowth first occurs from placodal neurons, but as gangliogenesis proceeds, neural crest cells also differentiate into N-cadherin-expressing neurons, and together both extend axons toward target tissues. However, a role for N-cadherin in regulating axon outgrowth and innervation of target tissues by trigeminal neurons has not been explored. To this end, we depleted N-cadherin from chick trigeminal placode cells and observed decreases in trigeminal ganglion size, nerve growth, and target innervation *in vivo*, phenotypes that could only partially be attributed to increased apoptosis early in gangliogenesis. Accordingly, neurite number and branching of neural crest-derived neurons was decreased *in vitro* in response to N-cadherin knockdown in placode cells, providing a novel non-cell autonomous explanation for these morphological changes. Inhibiting N-cadherin-mediated adhesion with a function-blocking antibody prevented axon extension in most, but not all, placode-derived trigeminal neurons *in vitro*, indicating potential unique requirements for N-cadherin in various neuronal subtypes. Collectively, these findings reveal persistent cell autonomous and non-cell autonomous functions for N-cadherin, thus highlighting the critical role of N-cadherin in mediating reciprocal interactions between neural crest and placode neuronal derivatives during trigeminal ganglion development.

INTRODUCTION

Sensory ganglia and their associated nerves transmit various inputs from the body and environment to the central nervous system[1]. These signals are detected by neurons whose cell bodies reside in the ganglia and whose axons project throughout the body where they facilitate diverse functions such as somatosensation and motility to visceral organs. Within the head, the cranial sensory ganglia perform these functions and are positioned along the roots of the cranial nerves. The trigeminal nerve, the largest and most complex of the twelve paired cranial nerves, relays the majority of somatosensory information within the head[2] and is composed of three major branches - the ophthalmic (OpV), maxillary (MxV), and mandibular (MnV) - that innervate the forehead and eye region, upper jaw, and lower jaw, respectively. While all three branches relay sensory information, only MnV has motor neurons that aid in mastication[3].

The chick embryo is an exemplary model for understanding developmental processes, including discerning the cell types that comprise the trigeminal ganglion[4,5]. Both neural crest cells and neurogenic placode cells differentiate into trigeminal sensory neurons[5], while the neural crest also gives rise to glial cells. Neural crest cells that contribute to the trigeminal ganglion originate from the midbrain and anterior hindbrain[6,7]; however, neural crest derivatives are found throughout the body axis as an array of cell types including cranial bone and cartilage, melanocytes, and cardiac myocytes[8,9]. Neurogenic placodes are specialized regions of thickened ectoderm that give rise to neurons within the cranial ganglia. Initially, there is slight overlap among them; however, as development progresses, they become more segregated and distinct[10]. While OpV and maxillomandibular (MmV) placodes comprise the trigeminal placode and generate one structure, they differ from one another in two important ways. First, they contribute neurons to distinct lobes of the trigeminal ganglion (OpV versus MxV or MnV, respectively). Second, OpV placode cells begin exiting the cell cycle and differentiating into neurons as early as E1/Hamburger-Hamilton stage (HH)8 and continue until E3.5/HH21[11], traveling to the trigeminal ganglion-forming region as a combination of neuroblasts and differentiated neurons. Conversely, the MmV placode generates neuroblasts that do not differentiate or become post-mitotic until they reach the ganglionic anlage[11–14]. Notably, in the chick, placodal neurons are the first neurons present within the trigeminal ganglion, differentiating and growing towards the periphery to make initial connections with their

targets within 2-5 days of development. In contrast, neural crest cells only begin neuronal differentiation at 4 days of development, and continue differentiating up to 7 days[4,15].

Reciprocal interactions between neural crest cells and placodal neurons are required to properly form the trigeminal ganglion[5,16,17]. The bulk of this research has focused on the influence of neural crest cells on surrounding cell types, but there is limited knowledge about how placodal neurons influence the neural crest. Because placodal neurons are present prior to neural crest-derived neurons, there is the intriguing possibility that they serve as pioneer neurons, the earliest population of neurons within a system that innervates targets, thereby providing a scaffold for later-born neurons to grow along[18]. Although supported by some studies[19,20], additional evidence for this is needed, and the molecules orchestrating this process remain unknown. However, intercellular adhesion among placode cells and neural crest cells regulates trigeminal gangliogenesis[21], and could therefore also function in facilitating trigeminal axon outgrowth to targets. Specifically, cadherins promote adhesion between adjacent cells and are known mediators of gangliogenesis[22–24]. The cadherin extracellular domain facilitates *cis* and *trans* interactions via homophilic and heterophilic binding[22,25,26] while the intracellular domain contains two binding sites for catenin proteins (p120-catenin and β-catenin) that regulate cadherin adhesive ability and provide a link to the actin cytoskeleton, respectively[27]. Neural cadherin (N-cadherin) is expressed in neural tissue at various stages of development[28], and in mesodermal[29,30] and ectodermal derivatives, including trigeminal and epibranchial placode cells prior to their delamination[23] and later in all trigeminal sensory neurons[31–34]. While multiple studies, largely in the central nervous system, describe roles for N-cadherin in regulating neurite formation[35–37], axon fasciculation[38], and synapse formation[39–41], the function of N-cadherin in sensory neurons has not been thoroughly characterized. Although N-cadherin function in placode cells is critical for the early condensation of the trigeminal ganglion from undifferentiated neural crest cells and placodal neurons[23], whether N-cadherin mediates the later growth and maturation of all trigeminal ganglion sensory neurons, and specifically neurite production and axon extension, is unknown. Furthermore, how N-cadherin-expressing placodal neurons impact the development of neural crest-derived neurons is poorly understood.

Building upon these prior studies, we demonstrate that placodal expression of N-cadherin is vital for later trigeminal neurodevelopment. We observed substantial deficits in trigeminal ganglion morphology and axonal projections to target tissues that arise from

effects on both placode- and neural crest-derived neurons in response to N-cadherin depletion from placodal neurons. These latter defects are noted both *in vivo* and *in vitro,* providing evidence to support the hypothesis that N-cadherin-mediated adhesion is important for trigeminal neurodevelopment. Strikingly, we note decreased neurite production in neural crest-derived neurons, indicating non-cell autonomous effects on the neural crest after N-cadherin knockdown in placodal neurons. These results indicate that trigeminal neurons depend on the adhesive function of N-cadherin to facilitate the outgrowth of axons. Altogether, our findings reveal a new long-term role for N-cadherin in driving the proper outgrowth of both placode- and neural crest-derived neurons throughout trigeminal gangliogenesis.

RESULTS

N-cadherin knockdown in placode cells disrupts trigeminal ganglion development

To elucidate the function of N-cadherin in placodal neurons during the formation and maturation of the trigeminal ganglion, a validated N-cadherin morpholino[23] (MO) was unilaterally electroporated into trigeminal placode cells at a single timepoint prior to their delamination. Embryos were grown to various endpoints ranging from 2.5-6.5 days of total incubation, then processed to assess morphological changes. Initial experiments with a 5 base pair mismatch N-cadherin control MO (N-cadherin MM)[23] were performed to compare electroporated and contralateral trigeminal ganglia to ensure the electroporation technique did not cause any morphological changes (Supplemental Figure 1). Once this was confirmed, the unelectroporated (contralateral) sides of N-cadherin MO-electroporated embryos were used as controls to account for any developmental variation. Trigeminal ganglion size and nerve morphology in electroporated embryos were analyzed at various developmental stages by whole-mount immunohistochemistry using an antibody against tubulin beta 3, class III (Tubb3) to label neurons, followed by tissue clearing to render samples transparent for imaging. Given the time difference in neuronal differentiation in the trigeminal ganglion[15,19], the Tubb3 antibody was presumed to identify placode-derived neurons up to E4/HH23, and labeled neuronal contributions from both cell types indistinguishably beyond this timepoint.

During initial gangliogenesis (E2.5/HH16-18), N-cadherin depletion from trigeminal placode cells led to more dispersed neurons and increased the area of the forming trigeminal ganglion compared to the unelectroporated contralateral side, which served as the control (Figure 1A-A', 1F). These results recapitulated previous work analyzing trigeminal ganglion area after N-cadherin knockdown in trigeminal placode cells, which found improper aggregation of trigeminal placodal neurons with each other and with undifferentiated neural crest cells in early gangliogenesis [23]. In contrast, following the condensation of the trigeminal ganglion 24 hours later in development (E3.5/HH19-22), we noted a statistically significant reduction in the size of the trigeminal ganglion on the electroporated side compared to the contralateral control (Figure 1B-B', 1F). This reduced size persisted even as neural crest cells began differentiating into neurons (Figure 1C-C', 1F; E4.5/HH23-25). Finally, at both E5.5/HH26-27 and E6.5/HH28-30, N-cadherin MO-electroporated trigeminal ganglia were no longer statistically different from unelectroporated contralateral trigeminal ganglia (Figure 1D-E', 1F).

Next, we measured the area of OpV and MmV individually. Interestingly, N-cadherin knockdown led to a statistically significant increase in MmV, but not OpV, at E2.5/HH16-18 (Figure 1G-H). However, throughout the remaining stages examined (E3.5-E6.5/HH19-30), N-cadherin depletion did not affect MmV lobe development (Figure 1H) but led to a statistically significant reduction in OpV lobe size (Figure 1D-D', 1G). At E6.5/HH28-30, the size of both lobes was not statistically different from unelectroporated contralateral lobes (Figure 1G-H). These findings point to potential cell (e.g., placode-derived neurons) and non-cell (e.g., neural crest-derived neurons) autonomous effects on trigeminal neurodevelopment. Given the disparate phenotypes associated with N-cadherin knockdown in OpV versus MmV (Figure 1G-H), we focused subsequent *in vivo* analyses on OpV development.

Depletion of N-cadherin from trigeminal placode cells disrupts target innervation by OpV nerves

Since extensive morphology changes were observed within the OpV lobe of the trigeminal ganglion, we next evaluated whether OpV axons and nerve projections into cranial target tissues might be impacted as well. We first examined the lateral nasal branch at E4.5/HH23-25, as by this point, the branch is a prominent structure within the embryonic head[42]. To this end, we performed whole-mount Tubb3 immunohistochemistry, which labels both placode- and neural crest-derived neurons at this stage, and compared the N-cadherin MO-electroporated side of the embryo to the unelectroporated contralateral side, which served as the control. These experiments revealed fewer lateral nasal nerve branches after N-cadherin MO treatment compared to the contralateral control side of the embryo (Figure 2A-B). To quantify these findings, we assessed the distribution of terminal nerve endings at 30 μm intervals across each image, starting at the first point in the image where axon branching occurred from the OpV lobe. More proximal to the trigeminal ganglion, there was no difference in the number of terminal nerve endings. In contrast, fewer were present in distal regions after N-cadherin MO treatment (Figure 2C). Moreover, nerve width and innervation area were significantly reduced after N-cadherin knockdown compared to the contralateral control (Figure 2D-E).

Using the same method, we evaluated the medial nasal nerve, which begins to form in E4.5/HH23-25 stage embryos[42]. Due to increased variability in this nerve at these stages, we examined the E5.5/HH26-27 timepoint to capture more consistent

morphological development. While the number of medial nasal terminal nerve endings was similar between conditions (Figure 2F-H), the nerve width and target innervation area were significantly smaller after N-cadherin knockdown compared to the unelectroporated contralateral control (Figure 2I-J). Together, these results reveal that N-cadherin is required by OpV trigeminal neurons to send axons to targets, thus leading to proper nerve outgrowth, fasciculation, and target innervation.

N-cadherin knockdown in placode cells leads to increased cell death within the OpV lobe

To assess whether altered OpV lobe size, axon outgrowth, and target innervation after N-cadherin knockdown in placode cells were due to cell death, a TUNEL assay was performed (Figure 3). Only the timepoints that showed significant differences in size from Figure 1 were examined (E2.5/HH16-18, E3.5/HH19-22, E4.5/HH23-25). Throughout these stages, apoptosis was evident in tissue sections from both the unelectroporated, contralateral control trigeminal ganglion (Figure 3A-A') and the N-cadherin MO-electroporated trigeminal ganglion (Figure 3B-B'). When correcting for size differences in the ganglion after N-cadherin knockdown, cell death was increased on the N-cadherin MO-treated side only during initial coalescence of placodal neurons with undifferentiated neural crest cells (E2.5/HH16-18), when OpV size is not changed (Figure 1A-A', 1G). Once placodal neurons and neural crest cells have formed the trigeminal ganglion, and neural crest cells have begun differentiating into neurons beyond E4, there was no significant difference in the TUNEL signal between the N-cadherin MO-treated and contralateral control sides (Figure 3C), even though OpV size was reduced at these stages after N-cadherin knockdown (Figure 1B-D', 1G). These findings suggest that apoptosis could partially account for some of the morphological phenotypes observed during early gangliogenesis prior to neural crest cell differentiation into trigeminal sensory neurons.

Neurite complexity in neural crest-derived neurons is reduced after N-cadherin knockdown in placode cells

Although we observed a slight increase in apoptosis, the absence of persistent apoptosis and presence of continued axon outgrowth deficits, particularly at stages when neural crest cells differentiate into neurons, led us to speculate that depletion of N-

cadherin from placode cells may be impacting later-born neural crest-derived neurons. To test this hypothesis, a sequential electroporation was performed using a genome-incorporating vector (PiggyBacGFP) and its accompanying transposase (PBase)[43,44] to first label neural crest cells with a stably expressed green fluorescent protein (GFP), followed by electroporation of placode cells with N-cadherin MO or the validated N-cadherin mismatch (MM) control morpholino (Supplemental Figure 1), which was used as the control for this experiment[23]. Sequentially-labeled trigeminal ganglia were dissected and cultured as explants, grown *in vitro* for 3 days, and subsequently processed for immunostaining with GFP and Tubb3 antibodies (Figure 4A). Remarkably, while N-cadherin MM-treated explant cultures exhibited numerous axons extending from neural crest-derived neurons (Supplemental Figure 2A-A'), qualitatively we observed relatively few GFP-positive neural crest-derived axons in N-cadherin MO-treated samples (Supplemental Figure 2B-B'). Interestingly, neurites, which precede axon specification and extension[45], were noted from GFP-positive neural crest-derived somata in both N-cadherin MO- and N-cadherin MM-treated explant cultures. While N-cadherin MM-treated explant cultures had numerous neurites per GFP-positive neural crest soma (Figure 4B-C), those in N-cadherin MO-treated explants had noticeably fewer (Figure 4D-E). Not only was there a significant decrease in the number of primary and secondary neurites in neural crest-derived neurons in N-cadherin MO-treated samples, but tertiary neurites were also absent even though they were observed in N-cadherin MM-treated explant cultures (Figure 4F). Although neurite branching was deficient in N-cadherin MO-treated explants cultures, there was no difference in the length of primary and secondary neurites compared to N-cadherin MM-treated explant cultures (Figure 4G). These results indicate that N-cadherin in placodal neurons non-cell autonomously facilitates extension and branching of axons in neural crest-derived neurons *in vitro*, providing an additional explanation for the sustained morphological deficits noted in the trigeminal ganglion.

N-cadherin controls proper axon outgrowth of trigeminal neurons *in vitro*

The morphological defects observed after N-cadherin knockdown in placode cells potentially point to a role for N-cadherin-mediated adhesion in facilitating axon outgrowth of both placode- and neural crest-derived trigeminal sensory neurons. If trigeminal placode-derived neurons express less N-cadherin, they may not properly adhere to each other, nor to N-cadherin-expressing neural crest-derived neurons, leading to deficiencies

in axon extension and target innervation. To test this, we utilized a validated function-blocking antibody against the extracellular domain of N-cadherin, known as MNCD2[32,46] (anti-N-cadherin), to block N-cadherin-mediated adhesion in explanted trigeminal ganglion tissue.

Trigeminal ganglion explant cultures were grown *in vitro* for 24 hours, then treated for 24 hours with anti-N-cadherin or a control rat IgG antibody (Figure 5A), followed by Tubb3 immunostaining (Figure 5B-C). Ridge detection processing of images was conducted to detect segments, which were used as a proxy for individual axons (Figure 5B', C'), and then an intersection analysis was run to measure changes to axon outgrowth (Figure 5B", 5C"). We observed a 53% reduction in the amount of Tubb3 fluorescence in the anti-N-cadherin-treated samples (Figure 5D), indicating decreased axon density in trigeminal ganglion explant cultures after blocking N-cadherin-based adhesion. Furthermore, our intersection analyses revealed a diminished number of axonal projections in the anti-N-cadherin-treated explant cultures up to 700 μm (Figure 5E). Interestingly, of the neurons that did extend axons, the average length of a single axon was similar between conditions (Figure 5F), signifying that some trigeminal neurons can properly extend axons independent of N-cadherin function. Collectively, these findings suggest N-cadherin-mediated adhesion promotes axonal outgrowth and complexity in trigeminal neurons *in vitro*, and that dependence on N-cadherin function may differ in distinct neuronal subtypes.

N-cadherin is required cell autonomously for the axon outgrowth of the majority of placodal neurons

Our preceding findings indicate that most trigeminal sensory neurons rely on N-cadherin for axon outgrowth. To investigate their cellular origin, an ectodermal co-electroporation with a stably expressed red fluorescent protein (PiggyBacRFP plus PBase)[43,44] was performed to label placode-derived neurons. Next, RFP-positive explant cultures were treated with either rat IgG or anti-N-cadherin as previously described. Following immunostaining with Tubb3 and RFP antibodies, robust axon outgrowth was observed, the majority of which overlapped with RFP-positive placode-derived neurons after rat IgG treatment (Figure 6A). Many Tubb3-positive projections were also RFP-positive in these control explant cultures (Figure 6B-B"). Explant cultures treated with anti-N-cadherin, however, had reduced overall axon outgrowth and fewer RFP-positive

projections (Figure 6C), as noted previously (Figure 5C). While colocalization of Tubb3 and RFP was maintained in the anti-N-cadherin-treated axonal projections, the total amount of outgrowth was less (Figure 6D-D”). Importantly, although overall Tubb3 fluorescence was reduced in the anti-N-cadherin-treated explant cultures, indicating fewer axons after blocking N-cadherin-mediated adhesion, there was no change in the total amount of RFP signal between the two treatment groups (Figure 6E). These findings reveal that blocking N-cadherin-mediated adhesion did not negatively affect the presence of placodal neurons, but instead functions to facilitate axon outgrowth.

Given these data and our prior results pointing to a role for N-cadherin in axon outgrowth, we hypothesized that anti-N-cadherin-treated explant cultures would have a greater amount of RFP signal within the core of the explanted tissue, which contains the majority of the neuronal cell bodies, due to the increased presence of placodal neurons unable to extend axons in the absence of N-cadherin-mediated adhesion. To address this, we evaluated the RFP signal found in axonal projections versus RFP signal remaining within the core of the explanted tissue (Figure 6F). While 33% of the total RFP signal came from axonal projections in rat IgG-treated explants, this dropped to 13% in anti-N-cadherin-treated explants. In contrast, 67% of the total RFP signal was found in the core of the rat IgG-treated explants versus 87% in anti-N-cadherin-treated explants (Figure 6G). Taken together, these data highlight a cell autonomous requirement for N-cadherin-mediated adhesion in the proper axon outgrowth of placode-derived neurons.

DISCUSSION

Here we demonstrate a sustained role for N-cadherin during trigeminal gangliogenesis that highlights the requirement of cell-cell adhesion during the formation and subsequent maturation of the OpV lobe of the trigeminal nerve. Our findings show that reducing N-cadherin from trigeminal placode cells and their neuronal derivatives leads to altered trigeminal ganglion morphology and deficient target innervation by specific OpV nerve branches. We found that N-cadherin-mediated adhesion is necessary for the outgrowth of the majority of placode-derived neurons, with neural crest-derived neurons relying upon N-cadherin in placodal neurons for proper neurite outgrowth. These results shed light on the continued role of N-cadherin for sensory neurodevelopment, and further confirm the importance of reciprocal interactions between placode cells and neural crest cells during cranial ganglia formation.

Depletion of N-cadherin from placodal neurons leads to persistent morphological defects in the developing trigeminal ganglion

Although N-cadherin in placode cells plays an important role during the initial coalescence of undifferentiated neural crest cells and placodal neurons to generate the trigeminal ganglion[23], whether N-cadherin further regulates the ability of trigeminal neurons to extend axons to properly innervate their targets has not been explored. Through our experiments, we showed that N-cadherin knockdown first increased ganglion area during early gangliogenesis, replicating previously published results[23], but then led to a reduction in trigeminal ganglion size up to 4.5 days into development, which eventually recovered. We believe there are two likely reasons for this recovery. First, MOs are typically only stable for up to 4-5 days *in vivo*, reflecting a limitation of our technique[47]. Therefore, it is possible that at the later timepoints, the MO was targeted for degradation, minimizing phenotypic effects. Second, continued differentiation of neural crest cells into neurons and glia beyond E4-5/HH24-27[4] may eventually compensate for this decrease in trigeminal ganglion size, and we would not be able to distinguish this based on Tubb3 immunostaining alone.

Two distinct placodes, OpV and MmV, contribute to the trigeminal ganglion, with each expressing specific genes and staggered neuronal differentiation[48,49]. In line with previous studies examining N-cadherin function[23], we observed more drastic phenotypes in OpV versus MmV trigeminal neurons. Although this could be due to the mosaic nature

of the electroporation, we suspect this difference is most likely attributed to MO dilution over time in MmV. OpV placode cells are the first to express neuron-specific markers and adopt a post-mitotic neuronal fate, some even before leaving the ectoderm[11], which would lead to more discernable phenotypes given the timing of electroporation. Conversely, MmV placode cells remain as proliferative neuroblasts until after delamination[11–13]. In the OpV lobe, E3.5/HH19-22 showed the greatest difference in size after N-cadherin depletion from placode cells. This timepoint coincides with when the majority of placodal neurons have initiated growth towards their target tissues[19], and few neural crest cells have differentiated into neurons, potentially explaining the more drastic phenotype at this stage. If N-cadherin promotes axon outgrowth, then its reduction in placode cells would negatively impact trigeminal neurodevelopment, as noted in our findings.

Reducing N-cadherin in placodal neurons impacts OpV nerve innervation patterns

Traveling away from the cell bodies housed in the trigeminal ganglion, we ascertained how N-cadherin knockdown in placodal neurons impacts OpV axon outgrowth to target tissues. We uncovered a requirement for N-cadherin in the lateral and medial nasal branches of OpV, with the former exhibiting more drastic changes upon N-cadherin MO treatment. We found decreases in terminal nerve branches, nerve width, and innervation area in the lateral nasal nerve while the medial nasal nerve exhibited similar trends for nerve width and innervation area, albeit to a lesser extent. Interestingly, there was no change in the number of terminal nerve branches in the medial nasal branch. This contrasting result - a smaller nerve bundle having similar axonal branching - suggests that N-cadherin functions to adhere individual axons with each other at medial nasal branch targets. Similar phenotypes after N-cadherin perturbations have been observed in other systems as well[34,50,51].

Although both OpV branches begin developing at similar stages[42], we chose to examine the E5.5/HH26-27 timepoint for the medial nasal nerve studies due to more consistency among embryos. While possible that the difference in the age of embryos evaluated could explain the varying results between the nerve branches, it is equally plausible that the proportion of N-cadherin-expressing placodal neurons is different in each branch since the contribution of neural crest- and placode-derived neurons to these nerve branches is not known. Additionally, the differences observed could be due to when the respective branches develop, as our results suggest that medial nasal branch

development occurs after the lateral nasal branch. If true, then early knockdown of N-cadherin would preferentially impact the lateral nasal nerve since it develops first. Alternatively, the mosaic nature of the electroporation technique may also explain these phenotypes.

N-cadherin in placodal neurons functions non-cell autonomously to control neurite production in neural crest-derived neurons

Given the alterations to trigeminal ganglion morphology, we first asked whether these phenotypes were due to increased apoptosis within the trigeminal ganglion. Although our Tubb3 whole-mount immunohistochemistry results do not show a size difference in OpV at the first timepoint examined (E2.5/HH16-18), our TUNEL analyses revealed a statistically significant increase in apoptosis at this timepoint. These findings could indicate that initially the same number of cells are present and contributing to the forming ganglion, but then some of those cells actively undergo apoptosis, reducing OpV size at later stages and adding to the long-term phenotypes seen in our studies. While these findings provide a partial explanation for N-cadherin MO-induced phenotypes, the absence of any increased apoptosis at later stages, particularly when neural crest cells are differentiating into neurons, suggested other mechanisms were involved.

To address this, we discerned whether the axon outgrowth of neural crest-derived neurons was affected in a non-cell autonomous manner. Fluorescent labeling of neural crest cells followed by reducing N-cadherin in placode cells via N-cadherin MO treatment revealed very few neural crest-derived axons (Supplemental Figure 2). We observed reduced neurite complexity after N-cadherin MO treatment, indicating non-cell autonomous effects on neural crest-derived neurons. These findings further demonstrate the continued importance of N-cadherin-mediated interactions throughout trigeminal gangliogenesis, now between placode- and neural crest-derived neurons. Interestingly, although fewer neurites were observed in N-cadherin MO-treated explants, neurite length did not differ from N-cadherin MM control-treated explants, suggesting that processes controlling neurite length are not altered in neural crest-derived neurons upon knockdown of N-cadherin in placode cells. These results demonstrate that a subpopulation of neural crest-derived neurons may not require N-cadherin in placodal neurons for axon outgrowth.

N-cadherin functions in the production of neurites for other peripheral neurons[35], and its concentrated localization at specific sites along the cell membrane precedes

neurite formation[37]. Depletion of N-cadherin from placodal neurons could prevent *trans* N-cadherin interactions between neural crest cells/neural crest-derived neurons and placodal neurons, perturbing neurite production in the former. Additionally, N-cadherin is involved in the maintenance of dendrites[34], leading to the possibility that neural crest-derived neurites are less stable upon N-cadherin knockdown in placodal neurons. Irrespective of the mechanism behind reduced neurite formation, it is likely that disruptions to the cytoskeleton play a role. Membrane-bound N-cadherin regulates the availability of both β-catenin and p120-catenin for binding and activating various signaling pathways[52]. If membranous N-cadherin expression in neural crest-derived neurons is altered after N-cadherin knockdown in placode cells, the typical intracellular signaling required to activate GTPases and other cytoskeletal remodeling proteins could be lost in neural crest-derived neurons, negatively impacting neurite production. Finally, interactions between cadherins and receptor tyrosine kinases at cellular membranes reportedly regulate each other[53], including those occurring between N-cadherin and Fibroblast Growth Factor receptors[36,54], which may be critical for the proper growth, maturation, and survival of neural crest-derived neurons. These interactions may be disrupted if N-cadherin levels are reduced, both in placode- and neural crest-derived neurons.

N-cadherin-mediated adhesion facilitates axon outgrowth of placode- and neural crest-derived trigeminal neurons

To elucidate whether the phenotypes seen *in vivo* could be explained by the loss of N-cadherin-dependent adhesion, we used a function-blocking antibody to broadly inhibit N-cadherin in trigeminal ganglion explant cultures. Analysis of the anti-N-cadherin *in vitro* experiments led to two major conclusions. First, our intersection analyses indicated reduced axon outgrowth and branching when N-cadherin adhesion is inhibited. Second, no significant differences were noted in the average segment length, used as a proxy for axons, when comparing controls to anti-N-cadherin-treated explants. This indicates that the subset of trigeminal neurons unaffected by blocking N-cadherin function can extend axons in the same manner as their control counterparts, suggesting N-cadherin is not important for the outgrowth of these neurons. These data recapitulate what was observed *in vivo* when examining OpV target innervation. In both instances, N-cadherin knockdown did not completely inhibit target innervation but instead reduced the number of axons successfully reaching target tissues. While this phenotype could be attributed to the

mosaic nature of the MO electroporation, our *in vitro* results now offer another potential explanation, in that some neurons are not reliant on N-cadherin for the outgrowth of their axons.

We next identified the cellular origin of the neurons that required N-cadherin-mediated adhesion for their outgrowth. We hypothesized that these neurons would be placode-derived since placode cell neuronal differentiation precedes neural crest cell differentiation within the trigeminal ganglion *in vivo*[15]. Our experiments showed reduced axon outgrowth in anti-N-cadherin-treated explants possessing RFP-labeled placodal neurons, recapitulating results from the anti-N-cadherin wildtype explant experiments and our observations *in vivo*. While it is possible that some of the RFP-labeled neurons initially grew out and then died, leading to the reduction in the number of neurons present, we do not believe this to be the case since a subset of neurons were always capable of growing out irrespective of when the anti-N-cadherin antibody was added to the explants. Although total levels of RFP were unchanged between treatments, very interestingly, the distribution of RFP observed within the core of the explants versus in extended axons was altered after treatment with the anti-N-cadherin antibody. Decreased RFP was detected in axonal projections after anti-N-cadherin treatment, with the majority of RFP signal coming from inside the cores. This indicates that N-cadherin promotes axon outgrowth, with its absence limiting the amount of RFP-positive placodal neurons capable of extending axons from the explant core.

Surprisingly, a small subset of RFP-positive placodal neurons exhibited axon outgrowth after anti-N-cadherin treatment, which could represent potential pioneer neurons of the trigeminal ganglion. While much of the evidence for pioneer neurons comes from invertebrate models[55–58], some evidence exists in vertebrates[59–61], including studies of trigeminal neurodevelopment in mice, which revealed that the first axons to leave the OpV lobe pave the way for secondary axons to reach their targets[20]. A similar phenomenon has also been observed in the chick trigeminal ganglion, where a few placode-derived neurons were observed to extend axons to the periphery, providing a path for later-born neurons to follow[19]. Collectively, these studies and our new data suggest that a subset of placodal neurons may be pioneers that serve as templates upon which other placode-derived neurons and later neural crest-derived neurons ("followers") extend axons[19]. This N-cadherin-independent (pioneer) and -dependent (follower)

outgrowth is reminiscent of mechanisms regulating migration in the facial branchiomotor neuron system[62].

CONCLUSION

In this study, we have shown a sustained negative impact on the trigeminal ganglion after N-cadherin is depleted from placodal neurons. Changes to the size of the trigeminal ganglion, as well as reduced axon outgrowth to target tissues, are observed at early stages of development as well as later stages when neural crest cells have differentiated into neurons. These morphological differences cannot be fully explained by increased apoptosis. In support of this, neurite production in neural crest-derived neurons is altered, pointing to a non-cell autonomous effect and indicating a requirement for N-cadherin in placodal neurons to facilitate axon outgrowth from placode- and neural crest-derived trigeminal neurons. Blocking N-cadherin-mediated adhesion *in vitro* reduces axon outgrowth from most placodal neurons, demonstrating a cell autonomous function for N-cadherin in this process. Collectively, our results add to the growing amount of evidence of the importance of reciprocal interactions between neural crest cells and placode cells during the formation of the cranial ganglia, and highlight a long-term, critical role for N-cadherin during trigeminal gangliogenesis that will likely be translatable to other cranial ganglia and vertebrate species.

MATERIALS AND METHODS

Chick embryos

Fertilized chicken eggs (*Gallus gallus*) were obtained from the Department of Animal and Avian Sciences at the University of Maryland (MD) and Centurion Poultry Incorporated (GA) and incubated at 37°C in humidified incubators on their sides. Embryos were incubated to reach desired Hamburger Hamilton (HH) stages based on times provided therein[63].

Morpholinos

To reduce N-cadherin protein expression, a validated lissamine-tagged translation-blocking morpholino antisense oligonucleotide (MO) against the *N-cadherin* transcript was used (GeneTools, LLC)[23], with a sequence of 5'-GCGGCGTTCCCGCTATCCGGCACAT-3'. For some control experiments, a 5 base pair mismatch N-cadherin control MO (N-cadherin MM) was used[23], with a sequence of 5'-GCGcCcTTCCCcCTATgCcGCACAT-3' (altered base pairs in lowercase). Both MOs were diluted with ultrapure water and 10% sucrose (in 1X phosphate-buffered saline (PBS)) and used at a final concentration of 500 μM.

In ovo unilateral placode electroporation

To target trigeminal placode cells prior to their delamination, a unilateral electroporation was performed at E1.75/HH10-11. The N-cadherin MO, N-cadherin MM, or a combination of PiggyBacRFP, a genome incorporating vector[64] (0.819 μg/μl), with PBase, its transposase (0.912 μg/μl), was expelled on top of the ectoderm on one side of the embryo using a fine glass needle. Next, a 30-gauge needle was used to puncture a small hole through the vitelline membrane so that electrodes could lay vertically above and below the ectoderm over which the MO/plasmid had been placed. Three, 9V pulses were delivered over 50 ms at 200 ms intervals. After electroporation, eggs were resealed with tape and parafilm and grown at 37°C to desired stages of interest. Due to the inherent variations that arise during normal development, even when embryos are staged identically, the contralateral side of the electroporated embryo was a more appropriate control and was used for all *in vivo* studies. Embryos were screened for successful MO electroporation based on the red fluorescence of the MO prior to collection and use in subsequent assays.

Sequential electroporation method

To target both cell populations that contribute to the trigeminal ganglion, a modified sequential electroporation[22] was utilized. Briefly, a unilateral neural tube co-electroporation was first performed on E1.5/HH9 using a combination of PiggyBacGFP (0.819 µg/µl) and PBase[65] (0.912 µg/µl). Two, 15V pulses were delivered over 30 ms at 200 ms intervals. The electroporated embryos were re-incubated until they reached E1.75/HH10-11, and then the placode cells on the same side of the embryo were electroporated with the N-cadherin MO or N-cadherin MM in the same manner as described above. After this second electroporation, eggs were resealed with tape and parafilm and grown at 37°C to desired stages of interest.

Immunostaining

Electroporated embryos were collected at desired stages of interest and fixed in 4% paraformaldehyde (PFA) overnight at 4°C with agitation. Following fixation, embryos were washed 3 x 10 minutes in 1X PBS and stored in 1X PBS at 4°C until further processing. Primary antibodies used included Tubb3 (Abcam ab78078, 1:500 for section, 1:250 for whole-mount), GFP (Abcam ab6662, 1:250), and RFP (Invitrogen MA5-15257, 1:250). Secondary antibodies used included goat anti-mouse IgG_1 594 (Invitrogen), and goat anti-mouse IgG_{2a} 555 or 647 (SouthernBiotech).

Tissue sections: Embryos were processed through an increasing sucrose gradient (5% and 15% sucrose (Fisher) in 1X PBS) at 4°C either overnight or until they sank to the bottom of the glass vials they were stored in. Next, they were processed through 7.5% gelatin (Sigma) in 15% sucrose and 20% gelatin in 1X PBS, both at 37°C, either overnight or until the embryos sank. Embryos were embedded in 20% gelatin, flash-frozen using liquid nitrogen, and stored at -80°C until ready for use. Embedded embryos were then cryo-sectioned at 12 µm on charged slides (VWR). Slide-mounted tissue sections were stored at -20°C until ready for use. For immunohistochemistry, slides were de-gelatinized by incubation in 1X PBS at 42°C for 15-20 minutes. Following 3 x 5-minute washes in 1X PBS, the slides were blocked with 10% heat-treated sheep serum (Sigma, HTSS) in PBST (Sigma, 1X PBS + 0.1% Triton X-100) at room temperature for 1-2 hours in a humidified chamber, then rinsed in PBST. Primary antibodies were diluted in PBST + 5% HTSS, added to the slides, covered with a glass coverslip (Fisher) to prevent sections

from drying out, and incubated overnight at 4°C. The following day, the coverslips were removed, and the slides were washed 4 x 30 minutes in PBST. Secondary antibodies were then diluted in PBST + 5% HTSS, added to the slides, covered with a glass coverslip, and incubated overnight at 4°C. The next day, slides were again washed 4 x 30 minutes in PBST and mounted with DAPI-fluoromount media (SouthernBiotech).

Standard whole-mount immunohistochemistry: Embryos were blocked with 10% HTSS in PBST for 2 hours at room temperature. Following a rinse with PBST, primary antibodies were diluted in PBST + 5% HTSS and incubated overnight at 4°C with agitation. The following day, the embryos were washed 4 x 30 minutes in PBST. Secondary antibodies were diluted in PBST + 5% HTSS and incubated overnight at 4°C with agitation. The next day, embryos were again washed 4 x 30 minutes in PBST and stored in 1X PBS at 4°C until they were either imaged or cleared (see below).

Modified whole-mount immunohistochemistry for iDISCO clearing: An adapted protocol was used based on methods from[66]. Fixed embryos were washed twice for 1 hour in 1X PBS and were then taken through an increasing methanol (MeOH, Pharmco in 1X PBS) gradient (50% (1 x 1 hour), 80% (1 x 1 hour), 100% (2 x 1 hour)), before they were bleached overnight in 5% H_2O_2 (Sigma) in 20% DMSO (Fisher)/MeOH at 4°C. The next day, samples were taken through the following series of washes: 2 x 1 hour in 100% MeOH, 2 x 1 hour in 20% DMSO/MeOH, 1 x 1 hour in 80% MeOH, 1 x 1 hour in 50% MeOH, 2 x 1 hour in 1X PBS, and 2 x 1 hour in 1X PBS + 0.2% Triton X-100. Samples were incubated overnight in 20% DMSO/0.3M glycine (Fisher) in 1X PBS + 0.2% Triton X-100 at 4°C. The next day, samples were blocked in 10% HTSS/10% DMSO/1X PBS + 0.2% Triton X-100 overnight at 4°C. Embryos were washed 2 x 1 hour in 0.2% Tween-20 (Sigma) in 1X PBS with 10 µg/ml heparin (Fisher, PTwH) at room temperature before primary antibodies were added and incubated for 72 hours at 4°C. Primary antibodies were diluted in 5% DMSO/5% HTSS/PTwH. Samples were washed in PTwH for 24 hours before secondary antibodies were added (diluted in the same manner as the primary antibodies), and samples were incubated with secondary antibodies for 48 hours at 4°C. Samples were then washed for 48 hours in PTwH before iDISCO clearing (see below).

Explant immunocytochemistry: Explant slides were washed once with 1X PBS, followed by fixation in 4% PFA for 1 hour at room temperature with agitation. Following fixation, slides were rinsed with 1X PBS and stored in 1X PBS at 4°C until ready for

immunocytochemistry. A hydrophobic perimeter was drawn around the slides to prevent dehydration of tissue using an ImmEdge Pen (Vector Laboratories), and explants were taken through blocking, primary antibody incubation, and secondary antibody incubation in the absence of coverslips as described in the tissue section methods. Slides were mounted with DAPI-fluoromount media (SouthernBiotech) and covered with a glass coverslip.

Tissue clearing

As embryos progress through development and tissue structures surrounding the trigeminal ganglion become more complex, visualization of the trigeminal ganglion after whole-mount immunohistochemistry becomes increasingly difficult. Therefore, clearing methods to render the tissues transparent were performed. At early stages (up to E3.5/HH22), the FRUIT[67] tissue clearing protocol was used, whereas later stages required iDISCO[66] tissue clearing. With both protocols, MO fluorescence was quenched during the clearing process.

FRUIT: Following the standard whole-mount immunohistochemistry protocol, embryos were progressed through increasing concentrations of fructose (35%, 40%, 60% and 80% w/v) in 8M urea (Sigma), 0.5% (v/v) alpha-thioglycerol (Fisher) dissolved in ultrapure water ("FRUIT buffer") for a minimum of 8 hours, up to 24 hours at room temperature, depending on the stage of the embryo. The time spent in a certain concentration of FRUIT buffer was determined based on how quickly the sample was rendered transparent. A sample was only moved up to the next FRUIT buffer once it had visibly changed transparency. The FRUIT cocktail, containing increasing concentrations of fructose, was made by first dissolving fructose in ultrapure water at 37°C. Once dissolved, the urea was added, and the solution was rocked at room temperature until fully dissolved. Lastly, alpha-thioglycerol was added, and buffers were stored at 4°C until use. Embryos were imaged in 60% or 80% FRUIT buffer (depending on the stage of the embryo) in glass-bottomed petri dishes (MatTek). Typically, embryos up to E3/HH19 were imaged in 60% FRUIT while older embryos were imaged in 80% FRUIT.

iDISCO: Following the modified whole-mount immunohistochemistry protocol, embryos were washed in 1X PBS + 0.2% Triton X-100 for a minimum of 48 hours. Samples were incubated in 50% (v/v) tetrahydrofuran (THF, Sigma) in water overnight in glass vials, making sure that over 90% of the vial was filled with the solution. The following day,

embryos were then incubated in 80% THF in water for one hour, followed by 2 x 1-hour incubations in 100% THF. Next, samples were incubated in 100% dichloromethane (Sigma) for 1-2 hours (or until they sank to the bottom of the vial). Lastly, embryos were incubated in dibenzyl ether (DBE, Sigma) overnight and imaged the following day in DBE. All steps, including embryo storage in DBE, were performed at room temperature. iDISCO-cleared embryos were imaged in a glass petri dish containing a custom chamber[66], which was printed in Terrapin Works, part of the School of Engineering at the University of Maryland.

TUNEL assay

To assess apoptosis, the *In Situ* Cell Death Detection Kit, Fluorescein (Roche) was used according to manufacturer's instructions. Briefly, following secondary antibody washes (4 x 30 minutes in PBST), slides were washed once for 30 minutes in 1X PBS. Slides were re-fixed with 4% PFA for 20 minutes at room temperature, followed by one 30-minute wash in 1X PBS. The TUNEL reaction mixture was added to the slides (75 µL per slide), and a glass coverslip was placed over them. Slides were incubated in the dark for 1 hour at 37°C. Next, the coverslips were removed, and the slides were washed 3 x 5 minutes in 1X PBS. Lastly, slides were mounted with DAPI-fluoromount media (SouthernBiotech).

Trigeminal ganglion explant assay

Wildtype E2/HH13-14 embryos were removed from eggs and stored on ice in 1X PBS until dissections. Trigeminal ganglia were dissected on a sylgard-coated dish by first bisecting the embryo and then carefully taking the area of the forming trigeminal ganglion, making sure to exclude the eye and neural tube. Explants were cultured on 2-well glass chamber slides (ThermoFisher) coated with Poly-L-Lysine (0.01% PLL, Sigma) and fibronectin (0.01%, Sigma). To make the coated slides, PLL (diluted in ultrapure water) was added to each chamber on the glass slides and incubated inside a biosafety cabinet for 30 minutes at room temperature. The PLL was removed, and slides were washed 3 times with water. Next, fibronectin (diluted in DMEM media (ThermoFisher)) was added to each chamber and incubated at 37°C for a minimum of 2 hours. The fibronectin solution was removed and slides were stored at 4°C until needed (for up to one week). Explants

were grown in DMEM media supplemented with N2 (1%, ThermoFisher) and Penicillin/Streptomycin (1%, Fisher). Explants for N-cadherin function-blocking antibody experiments (see below) were grown in the supplemented DMEM media mentioned above. Sequentially-labeled cells for N-cadherin MO- or MM-containing explant experiments were grown in Neurobasal media (ThermoFisher) supplemented with B27 (1%, ThermoFisher), N2 (0.5%, ThermoFisher), Glutamax (1%, ThermoFisher), Penicillin/Streptomycin (1%, ThermoFisher), and with nerve growth factor (ThermoFisher), brain-derived neurotrophic factor (Amgen), and neurotrophin-3 (Amgen), all at 50 ng/ml.

N-cadherin function-blocking antibody experiments

After 24 hours of incubation, fresh media containing either an antibody to block N-cadherin function, MNCD2 (anti-N-cadherin, Developmental Studies Hybridoma Bank, 0.1 µg/ml), or a normal rat IgG control (Santa Cruz Biotechnology, 1.6 µg/ml), replaced the initial explant plating media, and explants were incubated overnight. The following morning, the slides were briefly rinsed with 1X PBS, and then fixed in 4% PFA for one hour at room temperature. The explants were washed 3 times in 1X PBS, and then processed for immunocytochemistry.

Confocal imaging

All images were acquired with the LSM Zeiss 800 confocal microscope (Carl Zeiss Microscopy, Thornwood, NY, USA). Laser power, gain, and offset were kept consistent for the different channels during all experiments where possible. Fiji (NIH)[68] and Adobe Photoshop CC 2023 were used for image processing. For whole-mount imaging with Z-stacks, all embryos were imaged at a 5 µm interval. For sections, images of at least five serial transverse sections were acquired and used for analysis. For all experiments, a minimum of five replicates was obtained.

Quantifications and statistical analyses

Area measurement: For area measurements of the whole trigeminal ganglion, the OpV lobe, and the MmV lobes, maximum intensity Z-projections were first generated from Z-stacks taken through the trigeminal ganglion using Fiji. The polygon tool was used to outline the perimeter of Tubb3 signal and area measurements were generated. Individual

area measurements for each developmental stage grouping were averaged together and plotted to generate graphs in PRISM (GraphPad Software, Inc.)

TUNEL: N-cadherin MO-treated embryos were processed for section immunohistochemistry for Tubb3, followed by the TUNEL staining protocol. With the Tubb3 channel image, the polygon tool was used to trace the outline of the trigeminal ganglion. The outline was added to the region of interest manager, and then used to crop the TUNEL channel to only include the area of the image that contained neurons of the trigeminal ganglion. Once images from all experiments were processed, they were analyzed using the Squassh[69] plugin from the MOSAICsuite[70] in Fiji, as described[22]. Segmentation parameters were kept uniform for all images and run as a batch function. Following batch analysis, the quality of image segmentation was confirmed visually to ensure accurate segmentation. If batch parameters were not sufficient, they were adjusted on a case-by-case basis and the segmentation analysis was rerun. The number of puncta was calculated per image and averaged to obtain an average number per replicate, which was then divided by the average area of the trigeminal ganglion, to adjust for size differences. Individual averages for each developmental stage grouping were averaged together and plotted to generate graphs.

Nerve branching: Z-stack images of the OpV branch of the trigeminal nerve were analyzed in Fiji using custom ImageJ Macro language (IJM) scripts (available upon request). Maximum intensity Z-projection images were generated and inputted into the ImageJ macro. Signal profiles were obtained via successive vertical line selections using *getProfile()* at 30 μm intervals. The number of terminal nerve branches present at increasing distances from the starting point were exported and calculated in R (R core team, Vienna, Austria, 2021, scripts available upon request). Data for individual replicates for each condition were aligned so that quantification of nerve branching over a distance concordantly began with the first measurement found. Data were displayed as the mean quantity of nerve branches and plotted to generate graphs.

Nerve width: Using maximum intensity Z-projections, nerve width measurements for both the lateral and medial nasal nerves were generated using the straight line tool on Fiji. The width of individual OpV nerve divisions (prior to the point of extensive branching within the target tissue) was measured based on Tubb3 signal for each embryo. Widths were averaged for N-cadherin MO-treated embryos and their contralateral control sides and plotted to generate graphs.

Innervation area: Using maximum intensity Z-projections, innervation area measurements for both the lateral and medial nasal nerves were generated using the polygon tool on Fiji. A border was drawn around the Tubb3 signal in respective target tissues where terminal nerve branching occurred. Individual area measurements were averaged together for N-cadherin MO-treated embryos and their contralateral control sides, then plotted to generate graphs.

Intersection analysis following treatment with anti-N-cadherin: Each low magnification (5X), tiled image of the explants was imported into Fiji. Background was removed and the ridge-detection plug-in[71] was used to highlight axonal outgrowth to quantify axon length. Using the detected segment binary images and the concentric circle plugin, 20 concentric circles were overlayed on the explant, centered at the middle of the explant. The number of axonal intersections at each successive ring of increasing diameter was counted and plotted to generate graphs.

RFP-labeled placode cell analysis: Each low magnification (5X), tiled image of the Tubb3 channel was first inputted into Fiji and background was eliminated. A polygon selection feature was used to isolate the core of the explant from its associated axonal projections. The fluorescent intensity of RFP signal was collected for both the axonal projections and the core of the explants. The mean signal of the axons was divided by the mean signal for the core to generate a ratio. Individual ratios were averaged across treatments and compared between conditions.

Simple neurite tracer analysis: Each high magnification (40X) Z-stack of GFP-positive neural crest-derived neurons was opened on Fiji using the simple neurite tracer plugin[72,73]. Starting from the cell body, primary neurites were traced as paths. Neurites extending from primary neurites were added as branch points and termed secondary neurites. Any neurite branching off secondary neurites was marked as a tertiary neurite. Mean neurite number and mean neurite length of primary, secondary, and tertiary neurites were plotted as scatterplots.

ACKNOWLEDGMENTS

The authors would like to thank the National Institute of Dental and Craniofacial Research (R01DE024217) and the University of Maryland Graduate School for financially supporting this research. Additionally, we would like to thank Ms. Zoe Davidson and Ms. Reagan Armstrong for their technical assistance. All schematics were created with Biorender.com.

REFERENCES

1. Vermeiren, S., Bellefroid, E.J., and Desiderio, S. (2020). Vertebrate Sensory Ganglia: Common and Divergent Features of the Transcriptional Programs Generating Their Functional Specialization. Front Cell Dev Biol *8*, 587699. https://doi.org/10.3389/fcell.2020.587699.

2. Heimer, L. (1983). Cranial Nerves. In The Human Brain and Spinal Cord (Springer US), pp. 237–260. https://doi.org/10.1007/978-1-4684-0150-9_18.

3. Gambeta, E., Chichorro, J.G., and Zamponi, G.W. (2020). Trigeminal neuralgia: An overview from pathophysiology to pharmacological treatments. Mol Pain *16*, 1744806920901890. https://doi.org/10.1177/1744806920901890.

4. D'Amico-Martel, A., and Noden, D.M. (1980). An autoradiographic analysis of the development of the chick trigeminal ganglion. J Embryol Exp Morphol *55*, 167–182.

5. Hamburger, V. (1961). Experimental analysis of the dual origin of the trigeminal ganglion in the chick embryo. J. Exp. Zool. *148*, 91–123. https://doi.org/10.1002/jez.1401480202.

6. Noden, D.M. (1973). The migratory behavior of neural crest cells. Symp Oral Sens Percept, 9–36.

7. Lumsden, A., Sprawson, N., and Graham, A. (1991). Segmental origin and migration of neural crest cells in the hindbrain region of the chick embryo. Development *113*, 1281–1291. https://doi.org/10.1242/dev.113.4.1281.

8. Rodrigues-Da-Silva, M.A., De Espindola Da Silveira, G., Taufer, C.R., and Calloni, G.W. (2022). The mesenchymal potential of trunk neural crest cells. Int. J. Dev. Biol. *66*, 317–331. https://doi.org/10.1387/ijdb.220032gc.

9. Bronner, M.E., and LeDouarin, N.M. (2012). Development and evolution of the neural crest: An overview. Developmental Biology *366*, 2–9. https://doi.org/10.1016/j.ydbio.2011.12.042.

10. Bellairs, R., and Osmond, M. (2014). The atlas of chick development Third edition. (Elsevier/AP, Academic Press is an imprint of Elsevier).

11. McCabe, K.L., Sechrist, J.W., and Bronner-Fraser, M. (2009). Birth of ophthalmic trigeminal neurons initiates early in the placodal ectoderm. J of Comparative Neurology *514*, 161–173. https://doi.org/10.1002/cne.22004.

12. Graham, A., and Shimeld, S.M. (2013). The origin and evolution of the ectodermal placodes. Journal of Anatomy *222*, 32–40. https://doi.org/10.1111/j.1469-7580.2012.01506.x.

13. Begbie, J. (2002). Early Steps in the Production of Sensory Neurons by the Neurogenic Placodes. Molecular and Cellular Neuroscience *21*, 502–511. https://doi.org/10.1006/mcne.2002.1197.

14. Shiau, C.E., Das, R.M., and Storey, K.G. (2011). An effective assay for high cellular resolution time-lapse imaging of sensory placode formation and morphogenesis. BMC Neurosci *12*, 37. https://doi.org/10.1186/1471-2202-12-37.

15. D'Amico-Martel, A., and Noden, D.M. (1983). Contributions of placodal and neural crest cells to avian cranial peripheral ganglia. Am. J. Anat. *166*, 445–468. https://doi.org/10.1002/aja.1001660406.

16. Moody, S.A., and Heaton, M.B. (1983). Developmental relationships between trigeminal ganglia and trigeminal motoneurons in chick embryos. I. Ganglion development is necessary for motoneuron migration. J of Comparative Neurology *213*, 327–343. https://doi.org/10.1002/cne.902130308.

17. Shiau, C.E., Lwigale, P.Y., Das, R.M., Wilson, S.A., and Bronner-Fraser, M. (2008). Robo2-Slit1 dependent cell-cell interactions mediate assembly of the trigeminal ganglion. Nat Neurosci *11*, 269–276. https://doi.org/10.1038/nn2051.

18. Bate, C.M. (1976). Pioneer neurones in an insect embryo. Nature *260*, 54–56. https://doi.org/10.1038/260054a0.

19. Moody, S.A., Quigg, M.S., and Frankfurter, A. (1989). Development of the peripheral trigeminal system in the chick revealed by an isotype-specific anti-beta-tubulin monoclonal antibody. J of Comparative Neurology *279*, 567–580. https://doi.org/10.1002/cne.902790406.

20. Stainier, D.Y., and Gilbert, W. (1990). Pioneer neurons in the mouse trigeminal sensory system. Proc Natl Acad Sci U S A *87*, 923–927. https://doi.org/10.1073/pnas.87.3.923.

21. Steventon, B., Mayor, R., and Streit, A. (2014). Neural crest and placode interaction during the development of the cranial sensory system. Developmental Biology *389*, 28–38. https://doi.org/10.1016/j.ydbio.2014.01.021.

22. Halmi, C.A., Wu, C.-Y., and Taneyhill, L.A. (2022). Neural crest cell-placodal neuron interactions are mediated by Cadherin-7 and N-cadherin during early chick trigeminal ganglion assembly. F1000Res *11*, 741. https://doi.org/10.12688/f1000research.122686.2.

23. Shiau, C.E., and Bronner-Fraser, M. (2009). N-cadherin acts in concert with Slit1-Robo2 signaling in regulating aggregation of placode-derived cranial sensory neurons. Development *136*, 4155–4164. https://doi.org/10.1242/dev.034355.

24. Wu, C., and Taneyhill, L.A. (2019). Cadherin-7 mediates proper neural crest cell–placodal neuron interactions during trigeminal ganglion assembly. genesis *57*, e23264. https://doi.org/10.1002/dvg.23264.

25. Straub, B.K., Rickelt, S., Zimbelmann, R., Grund, C., Kuhn, C., Iken, M., Ott, M., Schirmacher, P., and Franke, W.W. (2011). E–N-cadherin heterodimers define novel adherens junctions

connecting endoderm-derived cells. The Journal of Cell Biology *195*, 873–887. https://doi.org/10.1083/jcb.201106023.

26. Basu, R., Duan, X., Taylor, M.R., Martin, E.A., Muralidhar, S., Wang, Y., Gangi-Wellman, L., Das, S.C., Yamagata, M., West, P.J., et al. (2017). Heterophilic Type II Cadherins Are Required for High-Magnitude Synaptic Potentiation in the Hippocampus. Neuron *96*, 160-176.e8. https://doi.org/10.1016/j.neuron.2017.09.009.

27. Niessen, C.M., Leckband, D., and Yap, A.S. (2011). Tissue organization by cadherin adhesion molecules: dynamic molecular and cellular mechanisms of morphogenetic regulation. Physiol Rev *91*, 691–731. https://doi.org/10.1152/physrev.00004.2010.

28. Hatta, K., and Takeichi, M. (1986). Expression of N-cadherin adhesion molecules associated with early morphogenetic events in chick development. Nature *320*, 447–449. https://doi.org/10.1038/320447a0.

29. Nakagawa, S., and Takeichi, M. (1997). N-cadherin is crucial for heart formation in the chick embryo. Dev Growth Differ *39*, 451–455. https://doi.org/10.1046/j.1440-169X.1997.t01-3-00006.x.

30. Dady, A., Blavet, C., and Duband, J.-L. (2012). Timing and kinetics of E- to N-cadherin switch during neurulation in the avian embryo. Dev. Dyn. *241*, 1333–1349. https://doi.org/10.1002/dvdy.23813.

31. Inuzuka, H., Redies, C., and Takeichi, M. (1991). Differential expression of R- and N-cadherin in neural and mesodermal tissues during early chicken development. Development *113*, 959–967. https://doi.org/10.1242/dev.113.3.959.

32. Redies, C., Inuzuka, H., and Takeichi, M. (1992). Restricted expression of N- and R-cadherin on neurites of the developing chicken CNS. J Neurosci *12*, 3525–3534. https://doi.org/10.1523/JNEUROSCI.12-09-03525.1992.

33. Itoh, K., Ozaki, M., Stevens, B., and Fields, R.D. (1997). Activity-dependent regulation of N-cadherin in DRG neurons: differential regulation of N-cadherin, NCAM, and L1 by distinct patterns of action potentials. J Neurobiol *33*, 735–748. https://doi.org/10.1002/(sici)1097-4695(19971120)33:6<735::aid-neu3>3.0.co;2-a.

34. Tan, Z.-J., Peng, Y., Song, H.-L., Zheng, J.-J., and Yu, X. (2010). N-cadherin-dependent neuron–neuron interaction is required for the maintenance of activity-induced dendrite growth. Proc. Natl. Acad. Sci. U.S.A. *107*, 9873–9878. https://doi.org/10.1073/pnas.1003480107.

35. Bixby, J.L., and Zhang, R. (1990). Purified N-cadherin is a potent substrate for the rapid induction of neurite outgrowth. J Cell Biol *110*, 1253–1260. https://doi.org/10.1083/jcb.110.4.1253.

36. Hansen, S.M., Berezin, V., and Bock, E. (2008). Signaling mechanisms of neurite outgrowth induced by the cell adhesion molecules NCAM and N-Cadherin. Cell. Mol. Life Sci. *65*, 3809–3821. https://doi.org/10.1007/s00018-008-8290-0.

37. Gärtner, A., Fornasiero, E.F., Munck, S., Vennekens, K., Seuntjens, E., Huttner, W.B., Valtorta, F., and Dotti, C.G. (2012). N-cadherin specifies first asymmetry in developing neurons. EMBO J *31*, 1893–1903. https://doi.org/10.1038/emboj.2012.41.

38. Masai, I., Lele, Z., Yamaguchi, M., Komori, A., Nakata, A., Nishiwaki, Y., Wada, H., Tanaka, H., Nojima, Y., Hammerschmidt, M., et al. (2003). N-cadherin mediates retinal lamination, maintenance of forebrain compartments and patterning of retinal neurites. Development *130*, 2479–2494. https://doi.org/10.1242/dev.00465.

39. Riehl, R., Johnson, K., Bradley, R., Grunwald, G.B., Cornel, E., Lilienbaum, A., and Holt, C.E. (1996). Cadherin Function Is Required for Axon Outgrowth in Retinal Ganglion Cells In Vivo. Neuron *17*, 837–848. https://doi.org/10.1016/S0896-6273(00)80216-0.

40. Benson, D.L., and Tanaka, H. (1998). N-Cadherin Redistribution during Synaptogenesis in Hippocampal Neurons. J. Neurosci. *18*, 6892–6904. https://doi.org/10.1523/JNEUROSCI.18-17-06892.1998.

41. Jontes, J.D. (2018). The Cadherin Superfamily in Neural Circuit Assembly. Cold Spring Harb Perspect Biol *10*, a029306. https://doi.org/10.1101/cshperspect.a029306.

42. Higashiyama, H., and Kuratani, S. (2014). On the maxillary nerve: The Maxillary Nerve in Vertebrates. Journal of Morphology *275*, 17–38. https://doi.org/10.1002/jmor.20193.

43. Lu, Y., Lin, C., and Wang, X. (2009). PiggyBac transgenic strategies in the developing chicken spinal cord. Nucleic Acids Research *37*, e141–e141. https://doi.org/10.1093/nar/gkp686.

44. Macdonald, J., Taylor, L., Sherman, A., Kawakami, K., Takahashi, Y., Sang, H.M., and McGrew, M.J. (2012). Efficient genetic modification and germ-line transmission of primordial germ cells using piggyBac and Tol2 transposons. Proc. Natl. Acad. Sci. U.S.A. *109*. https://doi.org/10.1073/pnas.1118715109.

45. Sainath, R., and Gallo, G. (2015). Cytoskeletal and signaling mechanisms of neurite formation. Cell Tissue Res *359*, 267–278. https://doi.org/10.1007/s00441-014-1955-0.

46. Bronner-Fraser, M., Wolf, J.J., and Murray, B.A. (1992). Effects of antibodies against N-cadherin and N-CAM on the cranial neural crest and neural tube. Developmental Biology *153*, 291–301. https://doi.org/10.1016/0012-1606(92)90114-V.

47. Bill, B.R., Petzold, A.M., Clark, K.J., Schimmenti, L.A., and Ekker, S.C. (2009). A Primer for Morpholino Use in Zebrafish. Zebrafish *6*, 69–77. https://doi.org/10.1089/zeb.2008.0555.

48. Stark, M.R., Sechrist, J., Bronner-Fraser, M., and Marcelle, C. (1997). Neural tube-ectoderm interactions are required for trigeminal placode formation. Development *124*, 4287–4295. https://doi.org/10.1242/dev.124.21.4287.

49. Lassiter, R.N.T., Stark, M.R., Zhao, T., and Zhou, C.J. (2014). Signaling mechanisms controlling cranial placode neurogenesis and delamination. Developmental Biology *389*, 39–49. https://doi.org/10.1016/j.ydbio.2013.11.025.

50. Reis, S.A., Thompson, M.N., Lee, J.-M., Fossale, E., Kim, H.-H., Liao, J.K., Moskowitz, M.A., Shaw, S.Y., Dong, L., Haggarty, S.J., et al. (2011). Striatal neurons expressing full-length mutant huntingtin exhibit decreased N-cadherin and altered neuritogenesis. Human Molecular Genetics *20*, 2344–2355. https://doi.org/10.1093/hmg/ddr127.

51. Shikanai, M., Nishimura, Y.V., Sakurai, M., Nabeshima, Y., Yuzaki, M., and Kawauchi, T. (2018). Caveolin-1 Promotes Early Neuronal Maturation via Caveolae-Independent Trafficking of N-Cadherin and L1. iScience *7*, 53–67. https://doi.org/10.1016/j.isci.2018.08.014.

52. Radice, G.L. (2013). N-Cadherin-Mediated Adhesion and Signaling from Development to Disease. In Progress in Molecular Biology and Translational Science (Elsevier), pp. 263–289. https://doi.org/10.1016/B978-0-12-394311-8.00012-1.

53. Chiasson-MacKenzie, C., and McClatchey, A.I. (2018). Cell–Cell Contact and Receptor Tyrosine Kinase Signaling. Cold Spring Harb Perspect Biol *10*, a029215. https://doi.org/10.1101/cshperspect.a029215.

54. Nguyen, T., and Mège, R.M. (2016). N-Cadherin and Fibroblast Growth Factor Receptors crosstalk in the control of developmental and cancer cell migrations. European Journal of Cell Biology *95*, 415–426. https://doi.org/10.1016/j.ejcb.2016.05.002.

55. Klose, M., and Bentley, D. (1989). Transient pioneer neurons are essential for formation of an embryonic peripheral nerve. Science *245*, 982–984. https://doi.org/10.1126/science.2772651.

56. Lin, D.M., Auld, V.J., and Goodman, C.S. (1995). Targeted neuronal cell ablation in the drosophila embryo: Pathfinding by follower growth cones in the absence of pioneers. Neuron *14*, 707–715. https://doi.org/10.1016/0896-6273(95)90215-5.

57. Hidalgo, A., and Brand, A.H. (1997). Targeted neuronal ablation: the role of pioneer neurons in guidance and fasciculation in the CNS of *Drosophila*. Development *124*, 3253–3262. https://doi.org/10.1242/dev.124.17.3253.

58. Clarke, A., McQueen, P.G., Fang, H.Y., Kannan, R., Wang, V., McCreedy, E., Buckley, T., Johannessen, E., Wincovitch, S., and Giniger, E. (2020). Dynamic morphogenesis of a pioneer axon in *Drosophila* and its regulation by Abl tyrosine kinase. MBoC *31*, 452–465. https://doi.org/10.1091/mbc.E19-10-0563.

59. Eisen, J.S., Myers, P.Z., and Westerfield, M. (1986). Pathway selection by growth cones of identified motoneurones in live zebra fish embryos. Nature *320*, 269–271. https://doi.org/10.1038/320269a0.

60. Ghosh, A., Antonini, A., McConnell, S.K., and Shatz, C.J. (1990). Requirement for subplate neurons in the formation of thalamocortical connections. Nature *347*, 179–181. https://doi.org/10.1038/347179a0.

61. Gong, Q., and Shipley, M.T. (1995). Evidence that pioneer olfactory axons regulate telencephalon cell cycle kinetics to induce the formation of the olfactory bulb. Neuron *14*, 91–101. https://doi.org/10.1016/0896-6273(95)90243-0.

62. Wanner, S.J., and Prince, V.E. (2013). Axon tracts guide zebrafish facial branchiomotor neuron migration through the hindbrain. Development *140*, 906–915. https://doi.org/10.1242/dev.087148.

63. Hamburger, V., and Hamilton, H.L. (1992). A series of normal stages in the development of the chick embryo. Developmental Dynamics *195*, 231–272. https://doi.org/10.1002/aja.1001950404.

64. Chen, F., and LoTurco, J. (2012). A method for stable transgenesis of radial glia lineage in rat neocortex by piggyBac mediated transposition. J Neurosci Methods *207*, 172–180. https://doi.org/10.1016/j.jneumeth.2012.03.016.

65. Wang, W., Lin, C., Lu, D., Ning, Z., Cox, T., Melvin, D., Wang, X., Bradley, A., and Liu, P. (2008). Chromosomal transposition of *PiggyBac* in mouse embryonic stem cells. Proc. Natl. Acad. Sci. U.S.A. *105*, 9290–9295. https://doi.org/10.1073/pnas.0801017105.

66. Renier, N., Wu, Z., Simon, D.J., Yang, J., Ariel, P., and Tessier-Lavigne, M. (2014). iDISCO: A Simple, Rapid Method to Immunolabel Large Tissue Samples for Volume Imaging. Cell *159*, 896–910. https://doi.org/10.1016/j.cell.2014.10.010.

67. Hou, B., Zhang, D., Zhao, S., Wei, M., Yang, Z., Wang, S., Wang, J., Zhang, X., Liu, B., Fan, L., et al. (2015). Scalable and DiI-compatible optical clearance of the mammalian brain. Front Neuroanat *9*, 19. https://doi.org/10.3389/fnana.2015.00019.

68. Schindelin, J., Arganda-Carreras, I., Frise, E., Kaynig, V., Longair, M., Pietzsch, T., Preibisch, S., Rueden, C., Saalfeld, S., Schmid, B., et al. (2012). Fiji: an open-source platform for biological-image analysis. Nature Methods *9*, 676–682. https://doi.org/10.1038/nmeth.2019.

69. Rizk, A., Paul, G., Incardona, P., Bugarski, M., Mansouri, M., Niemann, A., Ziegler, U., Berger, P., and Sbalzarini, I.F. (2014). Segmentation and quantification of subcellular structures in fluorescence microscopy images using Squassh. Nat Protoc *9*, 586–596. https://doi.org/10.1038/nprot.2014.037.

70. Shivanandan, A., Radenovic, A., and Sbalzarini, I.F. (2013). MosaicIA: an ImageJ/Fiji plugin for spatial pattern and interaction analysis. BMC Bioinformatics *14*, 349. https://doi.org/10.1186/1471-2105-14-349.

71. Steger, C. (1998). An unbiased detector of curvilinear structures. IEEE Trans. Pattern Anal. Machine Intell. *20*, 113–125. https://doi.org/10.1109/34.659930.

72. Arshadi, C., Günther, U., Eddison, M., Harrington, K.I.S., and Ferreira, T.A. (2021). SNT: a unifying toolbox for quantification of neuronal anatomy. Nat Methods *18*, 374–377. https://doi.org/10.1038/s41592-021-01105-7.

73. Ferreira, T.A., Blackman, A.V., Oyrer, J., Jayabal, S., Chung, A.J., Watt, A.J., Sjöström, P.J., and Van Meyel, D.J. (2014). Neuronal morphometry directly from bitmap images. Nat Methods *11*, 982–984. https://doi.org/10.1038/nmeth.3125.

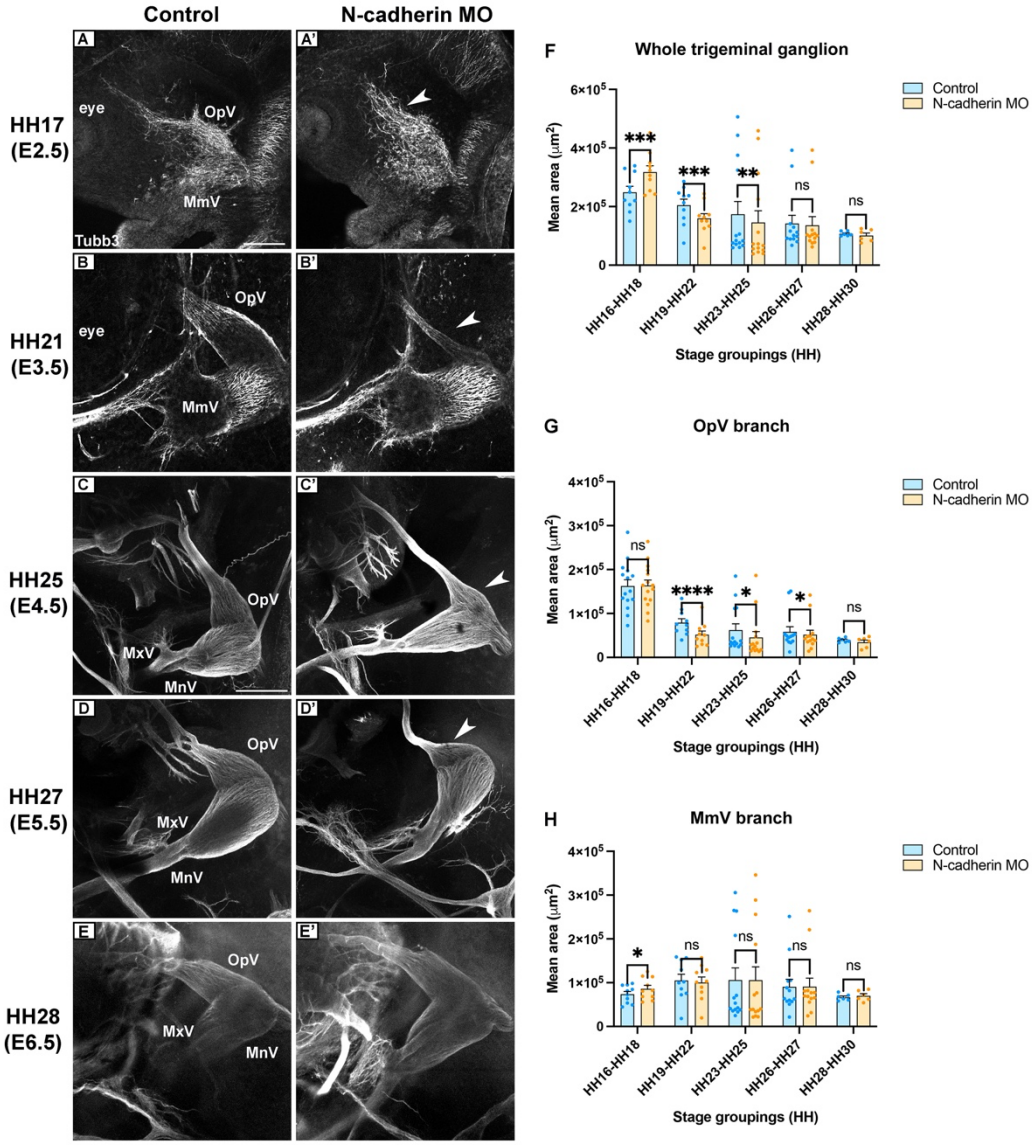

Figure 1. Knockdown of N-cadherin in placode cells disrupts trigeminal ganglion development. (A-E') Representative images of the trigeminal ganglion (contralateral control and N-cadherin MO-electroporated side) after immunostaining for Tubb3 and tissue clearing from various stage groupings (E2.5/HH16-18: A-A' (n=10), E3.5/HH19-22: B-B' (n=10), E4.5/HH23-25: C-C' (n=14), E5.5/HH26-27: D-D' (n=13), E6.5/HH28-30: E-E' (n=6)). Arrowheads highlight reductions in OpV lobe size in N-cadherin MO samples compared to controls. Scale bar in (A) is 250 μm and applies to (A'-B'). Scale bar in (C) is 250 μm and applies to (C'-E'). Mean whole trigeminal ganglia (F), OpV branch (G), and MmV/MxV branch (H) area ± SEM between contralateral and N-cadherin MO sides of embryos. Statistical significance was determined via paired t-tests. (*) $p<0.05$, (**) $p<0.01$, (***) $p<0.001$, (****) $p<0.0001$. Abbreviations: OpV: ophthalmic; MmV: maxillomandibular; MxV: maxillary; MnV: mandibular; ns: not significant.

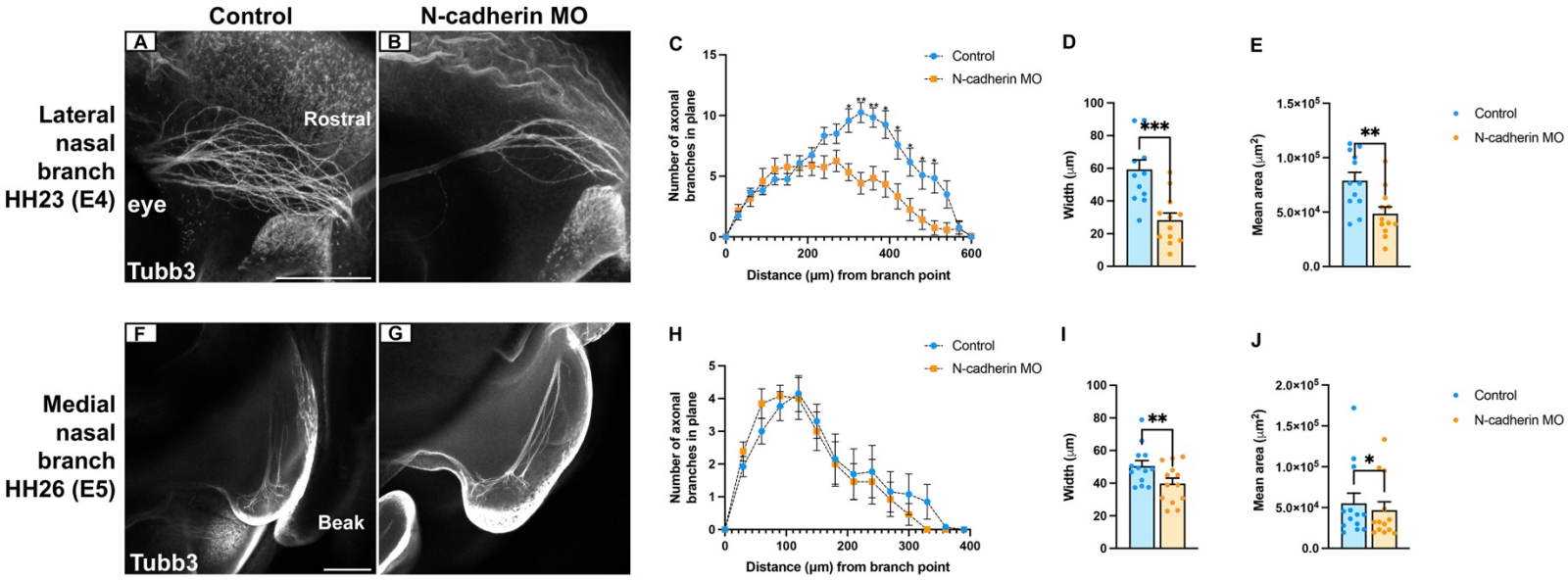

Figure 2. N-cadherin depletion from placode cells negatively impacts outgrowth and target tissue innervation for OpV nerve branches. (A, B, F, G) Representative images of the lateral (A, B) and medial (F, G) nasal nerves (contralateral control and N-cadherin MO-electroporated side) following immunostaining for Tubb3 and clearing with iDISCO (A, B: E4.5/HH23-25, n=12; F, G: E5.5/HH26-27, n=13, samples from whole-mounts were used in subsequent analyses). Scale bars in (A) and (F) are 250 μm and apply to (B) and (G), respectively. (C, H) Mean ± SEM of terminal nerve endings at increasing distances from the trigeminal ganglion. (D, I) Mean nerve width ± SEM calculated as a summation of the width of the nerve bundle prior to extensive axon branching. (E, J) Mean innervation area ± SEM calculated by measuring the area where axons terminate. Statistical significance was determined via paired t-tests (C-E, H-J), with adjustments made for multiple comparisons (C, H). (*) $p<0.05$, (**) $p<0.01$, (***) $p<0.001$.

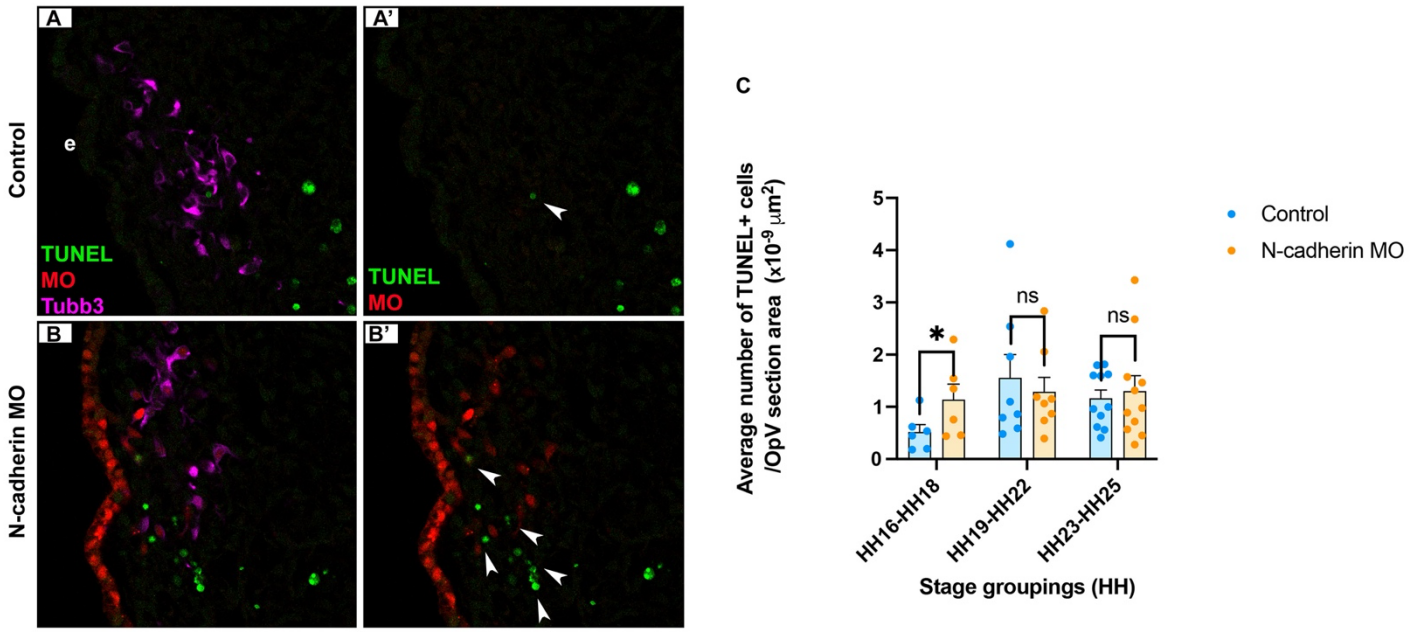

Figure 3. Morphological changes in the trigeminal ganglion after N-cadherin knockdown in placode cells are in part due to increased cell death (A-B') Transverse sections through the OpV lobe of the trigeminal ganglion (contralateral control and N-cadherin MO-electroporated side) from representative E2.25/HH16 embryos with immunostaining for Tubb3 and TUNEL staining. Scale bar in (A) is 50 µm and applies to all images. (C) Five serial sections per embryo from stage groupings E2.5/HH16-18 (n=6), E3.5/HH19-22 (n=8), and E4.5/HH23-25 (n=11) were imaged and used for analysis. Arrowheads in (A', B') mark TUNEL puncta. Statistical significance was determined via Wilcoxon signed-rank test. (*) $p<0.05$. Abbreviations: e, ectoderm; ns: not significant.

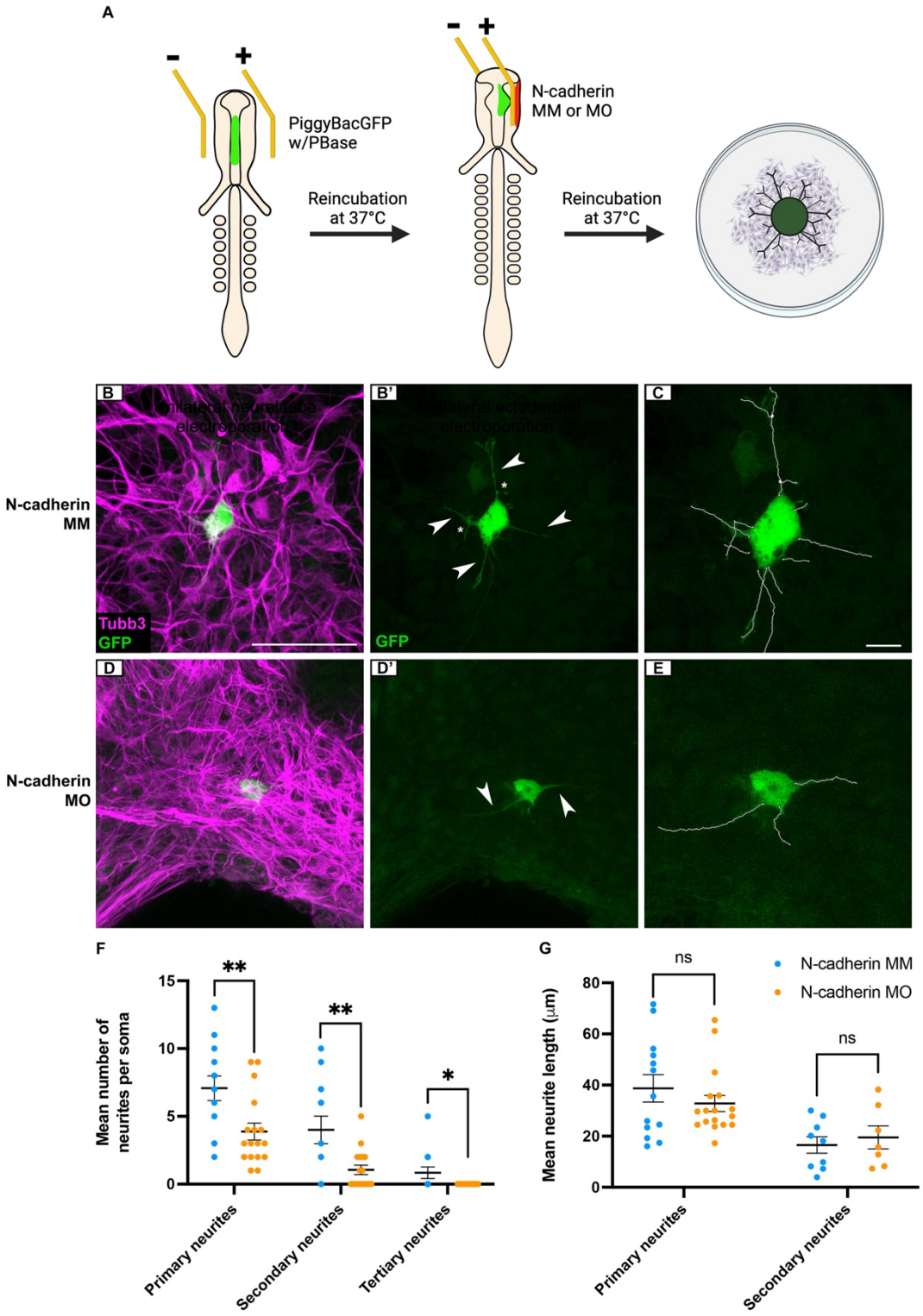
A
PiggyBacGFP
w/PBase
Reincubation
at 37°C
N-cadherin
MM or MO
Reincubation
at 37°C
B
B'
C
N-cadherin
MM
Tubb3
GFP
GFP
D
D'
E
N-cadherin
MO
F
Mean number of
neurites per soma
Primary neurites
Secondary neurites
Tertiary neurites
G
Mean neurite length (μm)
N-cadherin MM
N-cadherin MO
ns
ns
Primary neurites
Secondary neurites

Figure 4. N-cadherin depletion from placode cells decreases neurite complexity in neural-crest derived neurons. (A) Schematic of sequential electroporation explant culture technique. (B-E) Representative maximum intensity Z-projections of GFP-labeled neural crest-derived neurons after placodal electroporation with N-cadherin MM (B-B', n=13, control) or N-cadherin MO (D-D', n=17) taken from trigeminal ganglion explants following immunostaining for GFP and Tubb3, and neurite-traced images (C, E). Arrowheads and asterisks denote examples of primary and secondary neurites, respectively. Scale bar in (B) is 50 μm and applies to (B', D-D'). Scale bar in (C) is 10 μm and applies to (E). (F) Mean number ± SEM of GFP-positive neural crest-derived primary, secondary, and tertiary neurites after N-cadherin MM or N-cadherin MO electroporation. (G) Mean length ± SEM of GFP-positive neural crest-derived primary and secondary neurites after N-cadherin MM or N-cadherin MO electroporation. Statistical significance was determined via unpaired t-tests (D-E). (*) $p<0.05$, (**) $p<0.01$. ns: not significant.

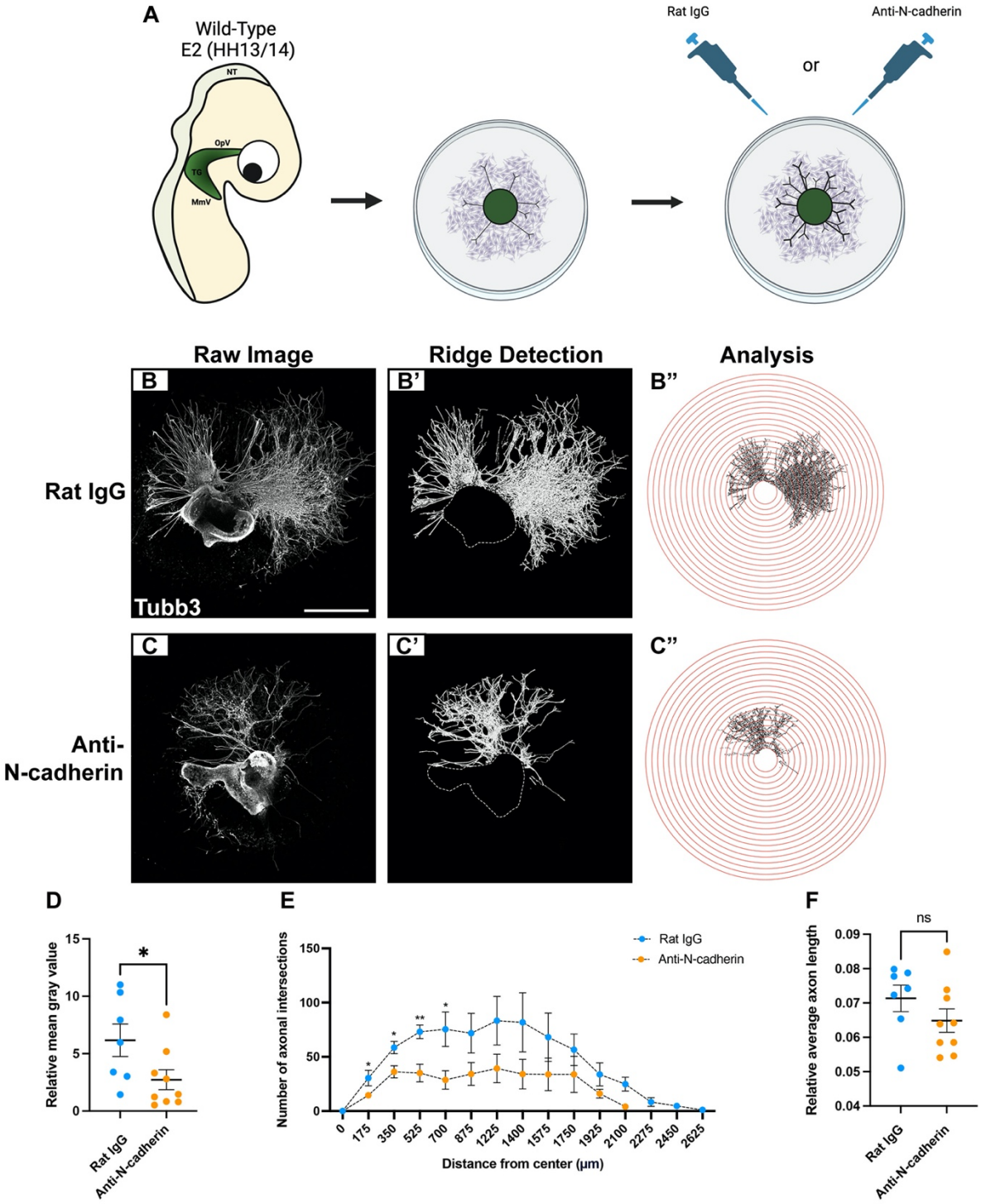
A
Wild-Type
E2 (HH13/14)
NT
OpV
TG
MmV
Rat IgG
or
Anti-N-cadherin
Raw Image
Ridge Detection
Analysis
B
B'
B''
Rat IgG
Tubb3
C
C'
C''
Anti-
N-cadherin
D
Relative mean gray value
Rat IgG
Anti-N-cadherin
E
Number of axonal intersections
Distance from center (µm)
Rat IgG
Anti-N-cadherin
F
Relative average axon length
ns
Rat IgG
Anti-N-cadherin

Figure 5. Blocking N-cadherin-mediated adhesion reduces trigeminal neuron axon outgrowth. (A) Schematic of N-cadherin function-blocking assay. (B-C') Workflow process for *in vitro* analyses. (B, C) Representative images of trigeminal ganglion explants after treatment with either control rat IgG (n=7) or anti-N-cadherin (n=9) antibody, respectively, followed by immunostaining for Tubb3. Scale bar in (B) is 1 mm and applies to (C). (B', C') Generated binary images after ridge detection processing on Fiji for rat IgG- or anti-N-cadherin-treated explants, respectively. Dotted lines indicate perimeter of explanted tissue that was cropped during processing. (B", C") Processed images overlaid with concentric circle function to count the number of axonal intersections at increasing intervals of 175 μm. (D) Mean signal intensity ± SEM of explant outgrowth following treatment with rat IgG or anti-N-cadherin, determined using ImageJ. (E) Intersection analysis calculating the number of axonal intersections across concentric circles of increasing diameter, presented as mean ± SEM. (F) Mean segment length ± SEM, where segments are considered as individual axons in each explant image after rat IgG or anti-N-cadherin treatment. Statistical significance was determined via unpaired t-tests (D-F) with adjustments made for multiple comparisons (E). (*) $p<0.05$.

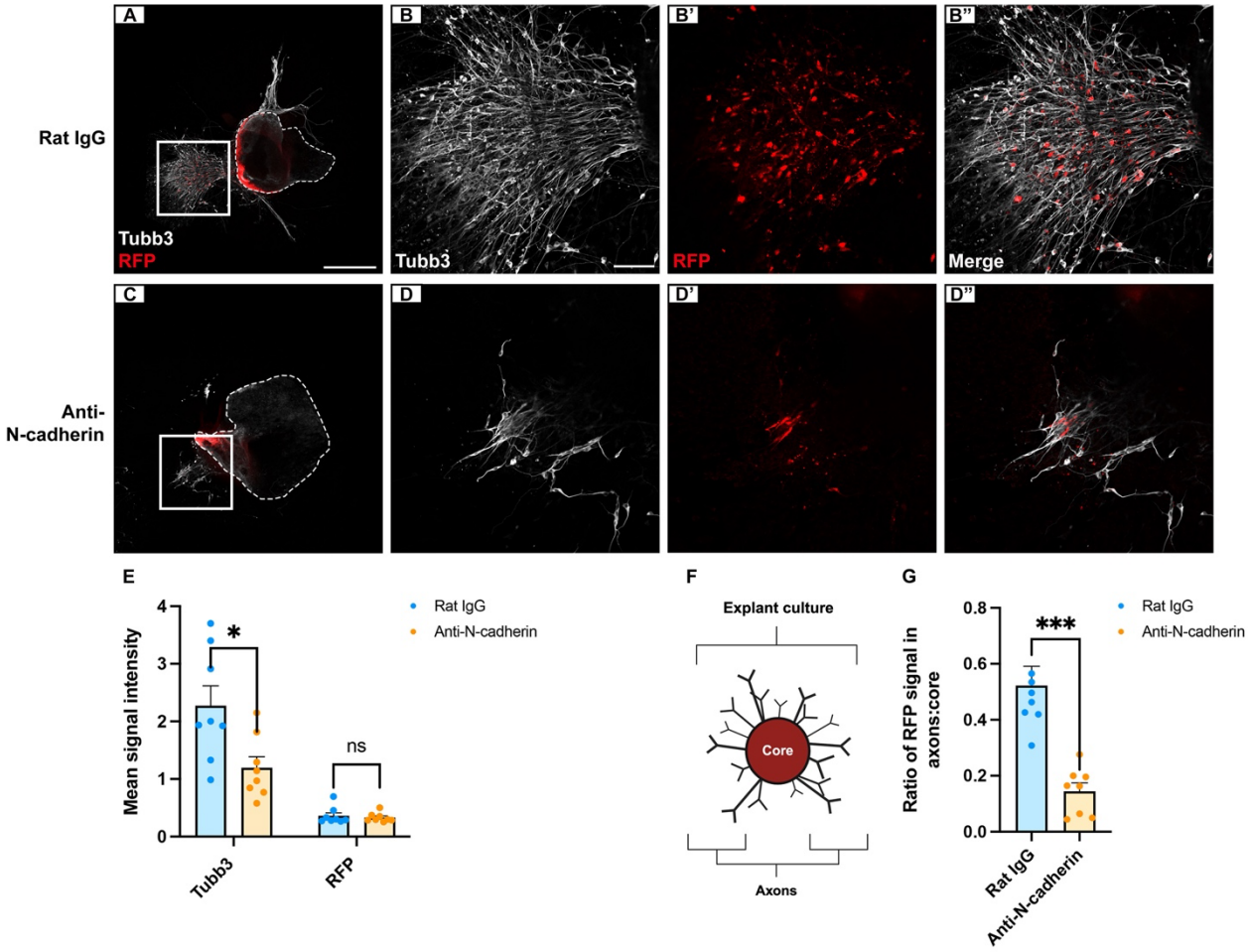

Figure 6. The majority of placodal neurons rely on N-cadherin for axon outgrowth. (A-D") Representative images of trigeminal explant cultures with RFP-labeled placodal neurons after control rat IgG (A-B", n=8) or anti-N-cadherin (C-D", n=8) treatment and immunostaining for RFP and Tubb3. Box in (A) and (C) indicates higher magnification images in (B-B"), and (D-D"), respectively. Dotted lines in (A) and (C) indicate perimeter of explanted tissue. Scale bar in (A) is 500 µm and applies to (C). Scale bar in (B) is 100 µm and applies to (B'-B", D-D"). (E) Mean signal intensity ± SEM for Tubb3 and RFP after rat IgG and anti-N-cadherin treatment. (F) Trigeminal ganglion explant culture schematic, with cores (found inside the explant) and axons (found outside the explant) comprising the explant culture. (G) Ratio of RFP signal found within axons and cores ± SEM. Signal intensity for RFP in axons was divided by signal intensity for RFP in cores for each condition (rat IgG and anti-N-cadherin) and presented as averages. Statistical significance was determined via the Mann-Whitney test (E, G) (*) $p<0.05$, (***) $p<0.001$.

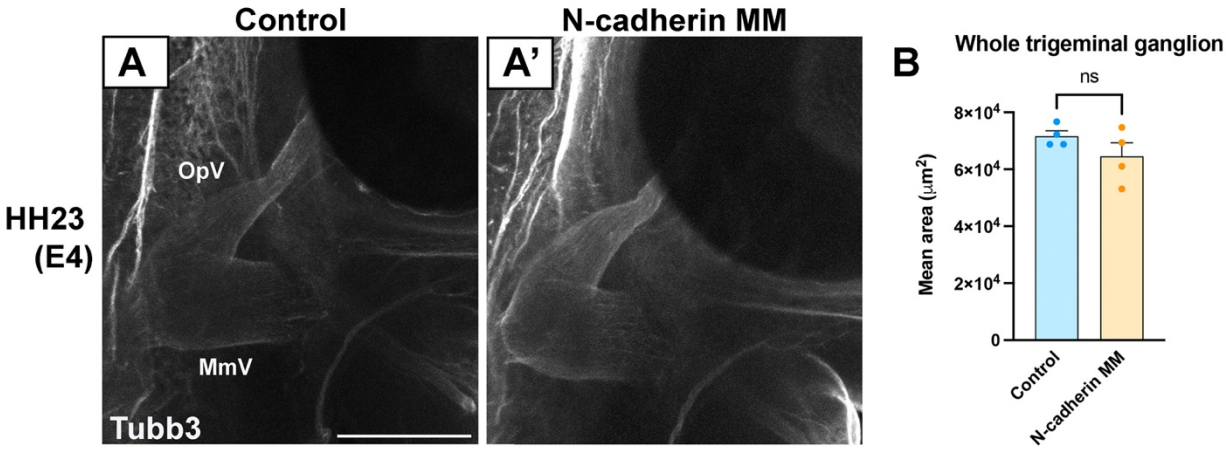

Supplemental Figure 1. N-cadherin mismatch control MO (MM)-treated embryos show no alterations in trigeminal ganglion morphology. (A-A') Representative images of the trigeminal ganglion after immunostaining for Tubb3 with iDISCO clearing (E4.5/HH23-25, n=4). Scale bar in (A) is 250 μm and applies to (A'). (B) Mean whole trigeminal ganglia area ± SEM between contralateral control and N-cadherin MM sides of embryos. Statistical significance was determined via a paired t-test. Abbreviations: OpV: ophthalmic; MmV: maxillomandibular; MM: mismatch control; MO: morpholino; ns: not significant.

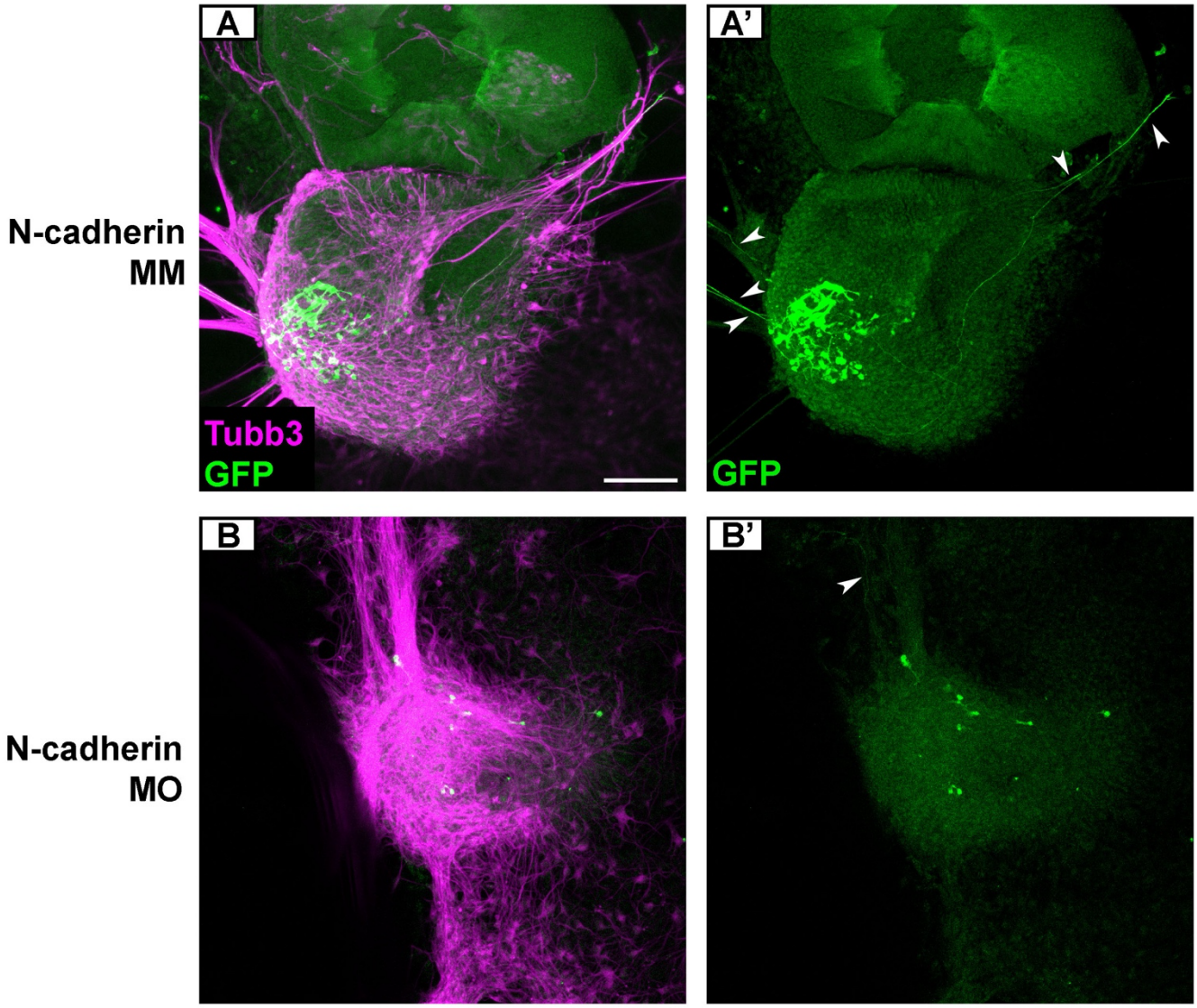

Supplemental Figure 2. N-cadherin MO-treated explants qualitatively exhibit less neural crest-derived axon outgrowth. (A-B') Representative images of sequentially electroporated trigeminal explants with neural crest cells co-electroporated with PiggyBacGFP plus PBase, and placode cells electroporated with N-cadherin MM (A-A') or N-cadherin MO (B-B'), followed by immunostaining for GFP and Tubb3. Scale bar in (A) is 100 μm and applies to all images. Arrowheads in (A') and (B') point to neural crest-derived axons.